Supporting information

Microwave shock-driven thermal engineering of unconventional cubic 2D $LaMnO_3$ for efficient oxygen evolution

Jiao Dai,‡[a] Mingjie Wang,‡[a,c] Haoran Tian,‡[a] Wenhui Fan,[a] Kaisi Liu,[a] Weilin Xu,[a] Huiyu Jiang,*[b] Huanyu Jin,*[c] and Jun Wan*[a]

[a] State Key Laboratory of New Textile Materials and Advanced Processing Technologies, School of Chemistry and Chemical Engineering, Wuhan Textile University, Wuhan 430200, China.

[b] School of Textile Science and Engineering, Wuhan Textile University, Wuhan 430200, China.

[c] Institute of Technology for Carbon Neutrality, Shenzhen Institute of Advanced Technology, Chinese Academy of Sciences, Shenzhen, 518055, China.

‡ These authors contributed equally to the work.

* **Correspondence to:** Prof. Jun Wan, State Key Laboratory of New Textile Materials and Advanced Processing Technologies, Wuhan Textile University, 1 Sunshine Avenue, Jiangxia District, Wuhan 430200, Hubei, China. E-mail: wanj@wtu.edu.cn;
Prof. Huiyu Jiang, School of Textile Science and Engineering, Wuhan Textile University, 1 Sunshine Avenue, Jiangxia District, Wuhan 430200, Hubei, China. E-mail: huiyujiang@wtu.edu.cn;
Prof. Huanyu Jin, Shenzhen Institute of Advanced Technology, Chinese Academy of Sciences, Shenzhen, 518055, China. E-mail: hy.jin2@siat.ac.cn

Supplementary Materials

1. Figure. S1 to S14

2. Table S1 to S3

1. Figure. S1 to S12

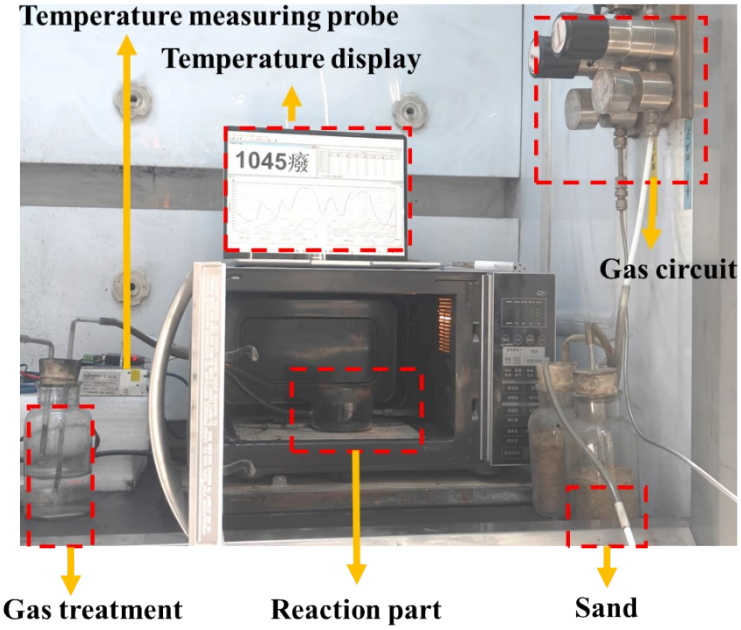

Fig. S1 Physical picture of microwave impact equipment.

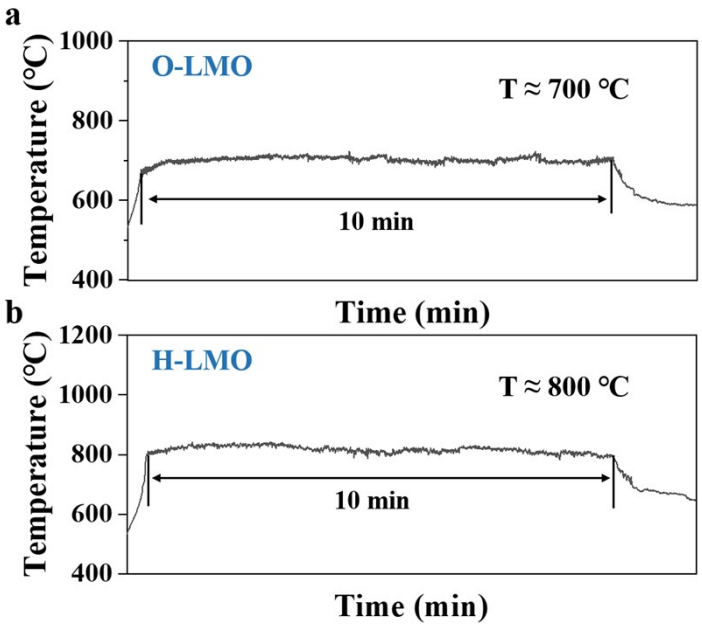

Fig. S2 Infrared real-time monitoring of O-LMO and H-LMO temperature map.

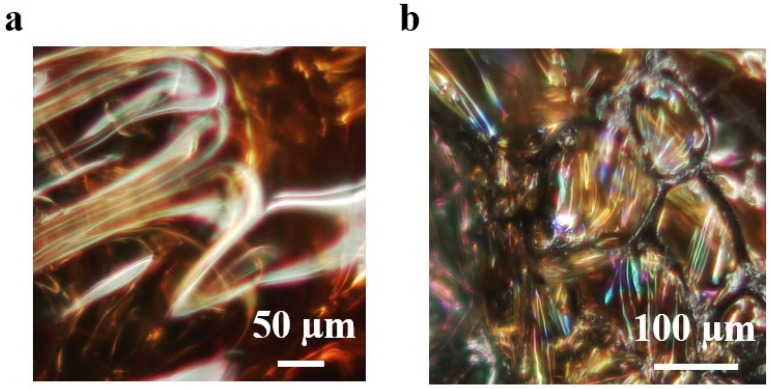

Fig. S3 Optical microscopy images during the synthesis process.

Fig. S4 Physical-optical photographs before and after the reaction.

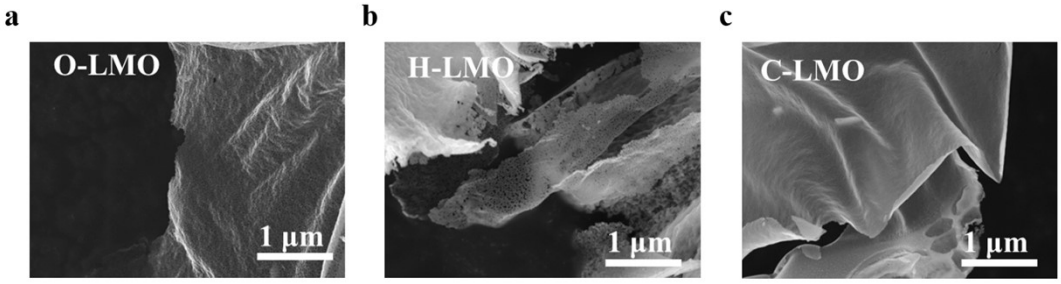

Fig. S5 SEM image of LMO.

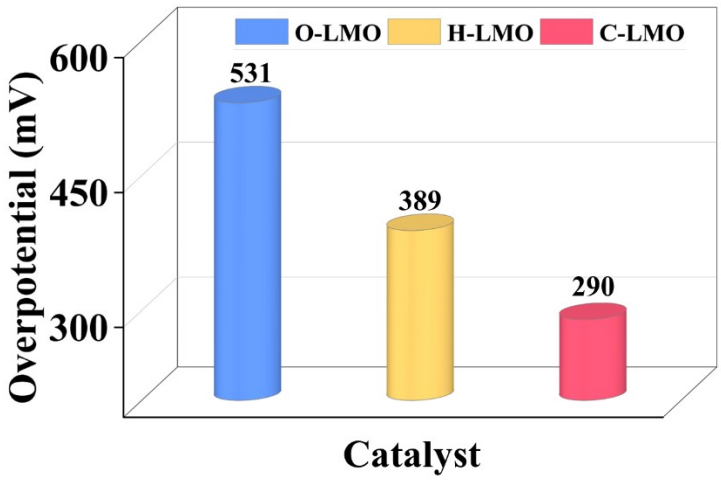

Fig. S6 Overpotential statistics of O-LMO, H-LMO, C-LMO.

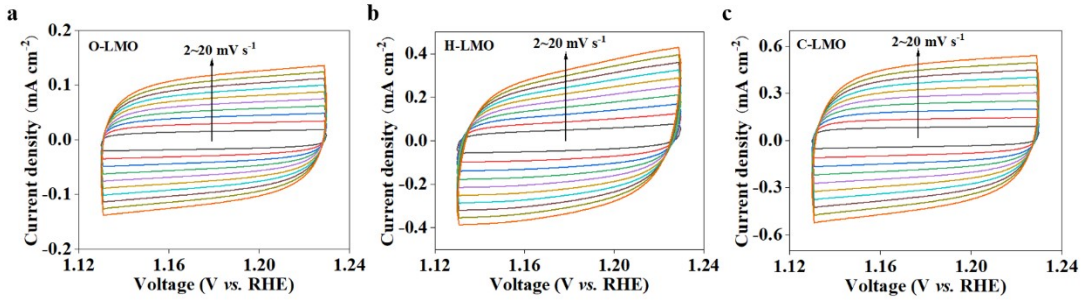

Fig. S7 CV measurements in a non-faradic current region (1.13-1.23V) at scan rates of 2 to 20 mV s^{-1} of (a) O-LMO, (b) H-LMO, (c) C-LMO in N_2-saturated 1.0 M KOH solution.

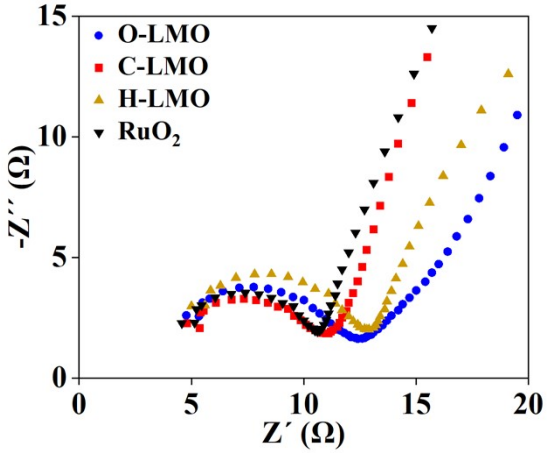

Fig. S8 Nyquist plots of O-LMO, H-LMO, C-LMO and RuO_2 catalysts.

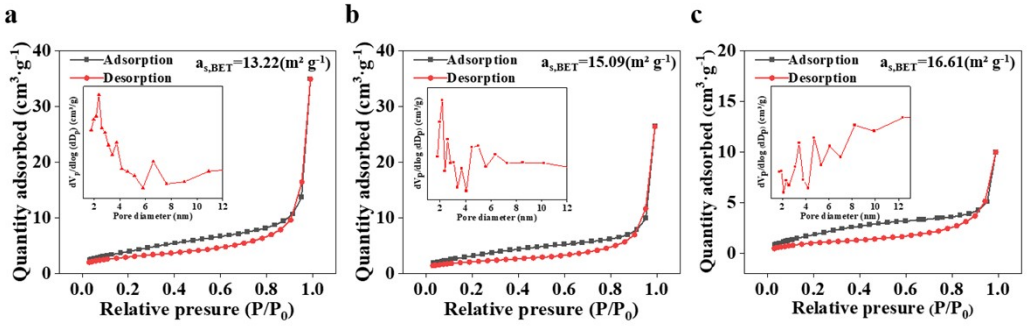

Fig. S9 BET diagram for (a) O-LMO, (b)H-LMO and (c) C-LMO.

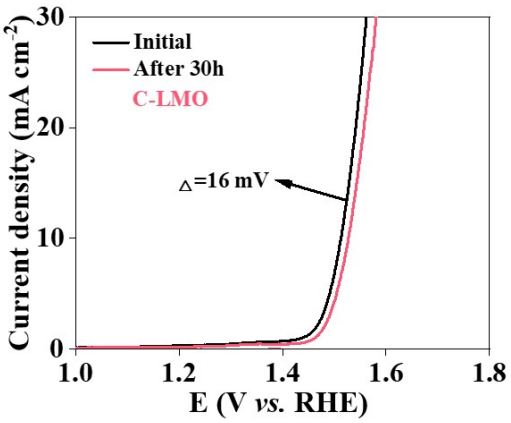

Fig. S10 The durability tests of C-LMO catalysts.

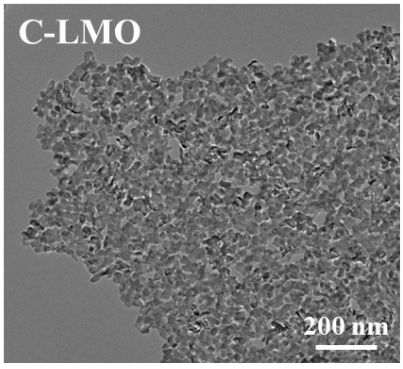

Fig. S11 TEM images of C-LMO catalysts after durability tests.

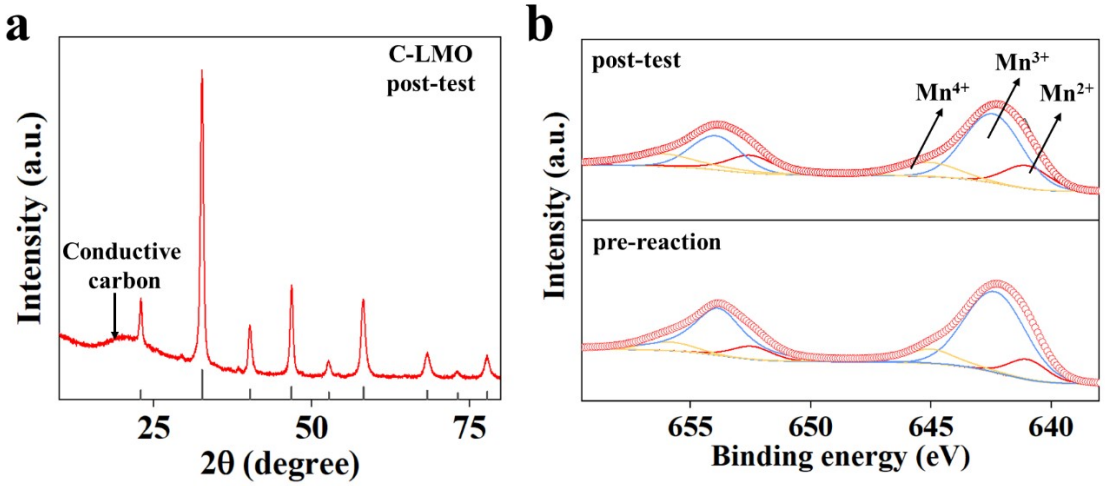

Fig. S12 (a) XRD features images of C-LMO catalysts after durability tests, (b) Mn 2*p* XPS Data before and after durability testing.

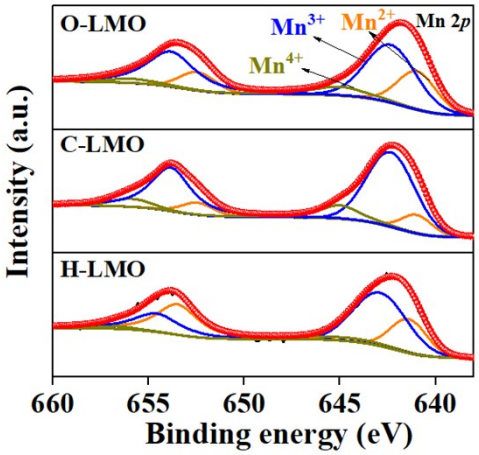

Fig. S13 High-resolution XPS spectra of Mn 2*p* features of O-LMO, H-LMO, C-LMO catalysts.

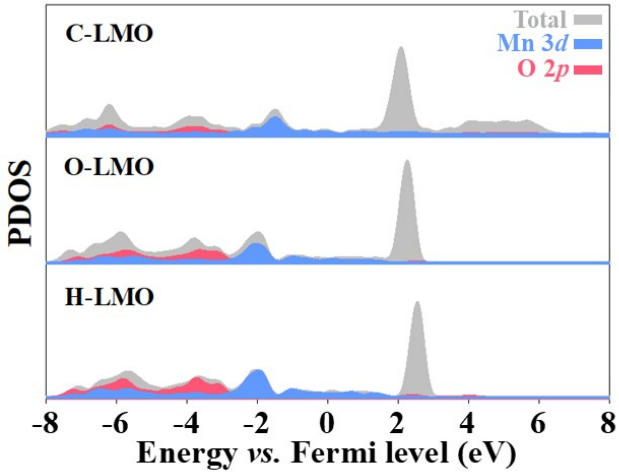

Fig. S14 Comprehensive PDOS for various elements in O-LMO, H-LMO, C-LMO catalysts.

2. Table S1 to S3

Table S1. The OER performance comparison of different catalysts.

	Electrocatalysts	Mass loading (mg cm^{-1})	Overpotential (mV vs. RHE)	Tafel slope (mV dec^{-1})	reference
This-work	C-$LaMnO_3$	0.52	290	66.21	This-work
Ref. 1	$LaCoO_3$	0.142	420	140	J. AlloysCompd. 2017, 725, 260.
Ref. 2	$LaFeO_3$	0.407	466	90	Angew. Chem. Int. Ed. 2019,18.
Ref.3	$NdFeO_3$	N/A	370	79	Int. J. Hydrogen Energy. 2022, 47, 14542.
Ref.4	$BaLa_2MnS_5$	N/A	338	108	J. Chin. Chem. Soc. 2024, 71, 1008.
Ref.5	$LaNiO_3$/C	0.250	426	119	Chem. 2019, 7, 2019.
Ref.6	$LaCoO_3$	N/A	470	180	Chem. 2017. 3. 812.
Ref.7	$LaFeO_3$	0.255	430	157	ACS Appl. Mater. Inter. 2020, 12, 4125963
Ref.8	$La_{0.6}Sr_{0.4}CoO_{3-\delta}$	N/A	420	99	Electrochim. Acta. 2019, 327, 135033 49
Ref.9	$LaCoO_3$	0.25	450	144	Energy Storage Mater. 2021, 42, 470 68
Ref.10	$SrCo_{0.9}Ru_{0.1}O_{3-\delta}$	N/A	360	113	Small 2019, 15, 1903120

Table S2. Parameters of LMO from Rietveld refinement.

	O-LMO	H-LMO	C-LMO
χ^2	1.91	1.98	1.90
R_{wp}	5.23%	4.23%	5.0%
R_P	3.84%	3.08%	3.75%

Table S3. Detailed lattice parameters of O-LMO, H-LMO and C-LMO.

		O-LMO	H-LMO	C-LMO
Space group		Pnma	R-3c:H	Pm-3m
Lattice parameters	a	5.565Å	5.529Å	3.887Å
	b	8.031Å	5.529Å	3.887Å
	c	5.563Å	13.366Å	3.887Å
	α	90°	90°	90°
	β	90°	90°	90°
	γ	90°	120°	90°
	V(Å^3)	248.678Å^3	353.949Å^3	58.763Å^3